Sensors and Actuators B 146 (2010) 165–170

Contents lists available at ScienceDirect

Sensors and Actuators B: Chemical

journal homepage: www.elsevier.com/locate/snb

# $WO_3$-based $NO_2$ sensors fabricated through low frequency AC electrophoretic deposition

Elham Kamali Heidari[a], Cyrus Zamani[b,*], Ehsan Marzbanrad[a], Babak Raissi[a], Soroush Nazarpour[c]

[a] Ceramic Department, Materials and Energy Research Center, Tehran, Iran
[b] ME2, XaRMAE, Department Electrònica, Universitat de Barcelona, Martí i Franquès 1, 08028 Barcelona, Spain
[c] MIND/IN2UB, Departament d'Electrònica, Universitat de Barcelona, Martí i Franquès 1, 08028 Barcelona, Spain

ARTICLE INFO

*Article history:*
Received 14 October 2009
Received in revised form 7 December 2009
Accepted 4 January 2010
Available online 16 February 2010

*Keywords:*
$NO_2$ sensor
Mesoporous $WO_3$
Low frequency electrophoretic deposition
Sensitivity

ABSTRACT

Mesoporous tungsten oxide was synthesized based on hard template method using silica as template. The produced material was investigated structurally using X-ray diffraction and high resolution TEM. The material was deposited on patterned alumina substrates through low frequency AC electrophoresis of which, the deposition pattern was studied using optical microscopy and SEM. Exposure of the sensors to $NO_2$ in the temperature range of 150–300 °C resulted in highest sensitivity at 200 °C. Increasing temperature was found to produce faster response and recovery processes while the sensitivity decreased.



## 1. Introduction

Exhaust gases generated by cars and factories are the focus of many researches as the main source of air pollution. NOx (NO, $NO_2$) as a toxic is of great importance and many researchers have reported metal oxide based sensors for NOx detection. Based on American standards, concentration of NO and $NO_2$ should not exceed 3 and 25 ppm respectively while in Japan, these fall in ppb range. Thus, there is an increasing need to highly sensitive sensors targeting NOx. A great number of sensors are reported so far with their advantages and drawbacks [1,2]. Solid-state NOx sensors reported so far can be categorized in several groups among which, resistive-type (based on semiconducting oxides), amperometric- and potentiometric-type (based on solid-electrolyte materials), and capacitive-type are of great importance. Combined structures are also reported presenting a combination of the properties of individual elements used in their structure [3–6]. Although a large number of works have been focusing on solid-electrolyte sensors which show a high sensitivity at elevated temperatures, progress in oxide materials and their novel structures is the motivation for research on resistive-sensors which operate at lower temperatures and benefit a simple structure. $SnO_2$, $In_2O_3$, $TiO_2$, ZnO, $Fe_2O_3$, $WO_3$ and several combinations of these (in some cases doped with a catalytic material) have been studied so far [7–13]. Of the oxide materials used for sensing, $WO_3$ shows promising properties especially if possesses a large surface area [14]. In this scenario, mesoporous materials are so far one of the best candidates presenting a high sensitivity thanks to their large specific surface area. The possibility of manipulating mesoporous materials with desired structural features is an advantage which makes the products suitable for sensing gases like amines which are difficult to be sensed by other structures [15,16].

On the other hand, the deposition process affects the device performance largely since it affects the morphology and structure of the sensing material (and thus, its properties) [17]. Thus, various deposition methods have been implemented such as melting and quenching [4,5], micro dropping [15,18], dip coating [19], screen printing [12], sputtering [10], etc. Low frequency electrophoresis is a method with high potentiality to deposit nanomaterials in a controlled way [20–23]. In this article, we present the application of low frequency AC electrophoretic deposition in sensor fabrication where $WO_3$ nanopowder is deposited on interdigitated electrodes. Fabricated devices are exposed to various concentrations of $NO_2$ for which, results are presented.

## 2. Experimental

### 2.1. $WO_3$ nano particles synthesis

Mesoporous $SiO_2$ was synthesized, as a template for impregnation of $WO_3$ nano particles based on method reported earlier [24,25]. A solution of 6 g polyethylene oxide–polypropylene oxide

* Corresponding author. Tel.: +34 934039174; fax: +34 934021148.
*E-mail address:* cyrus_zamani@yahoo.com (C. Zamani).

0925-4005/$ – see front matter © 2010 Elsevier B.V. All rights reserved.
doi:10.1016/j.snb.2010.01.073

block copolymer (Clariant PF-10), 180 ml distilled water and 30 g HCl (35 wt%) was made and stirred for 6 h at 35 °C. Then, we added tetraethyl orthosilicate (TEOS, Aldrich) to the resulting acidic solution and stirred it for 24 h at the same temperature. As the hydrothermal treatment, the solution was then heated at 100 °C for another 24 h. pH was maintained constant at 7 by addition of $NH_3$. Mesoporous silica was obtained by drying the resultant product in air atmosphere followed by 4 h calcination at 550 °C.

Phosphotungestic acid hydrate (merck #art no. B684983) and mesoporous $SiO_2$ were added to ethanol with the same ratio (1:1 by weight). The mixture was stirred for 1 h and dried at room temperature in air atmosphere. Calcination phase was performed at 570 °C with heating rate of 10 °C/min for 5 h (dwell time). At last, the $SiO_2$ hard template was removed by HF (2 wt%) and $WO_3$ was collected by centrifugation. The product was copiously washed with water and ethanol and finally dried at 100 °C. HRTEM (JEOL 2100), XRD (Siemens D500, Cu Kα radiation), and BET (BELsorp mini II) were employed for characterization of the synthesized material.

### 2.2. Sensor fabrication

Low frequency AC electrophoresis [20–22] was applied for deposition of $WO_3$ nano powders on an alumina substrate with interdigitated electrodes (with a spacing of about 100 μm). In the first step, a stable solution (suitable for electrodeposition) was prepared through making a suspension of 0.5 g/L $WO_3$ nanoparticles in acetone altrasonicated for 15 min. Deposition was performed by applying 30 V pick-to-pick square wave with 10 kHz frequency. Deposition time was 60 min. The resulting pattern was analyzed using optical microscopy and SEM (Stereo Scan 360-Leica/Cambridge) before exposing the device to the gas for sensing measurements.

## 3. Results and discussion

N2 adsorption/desorption isotherm of synthesized silica (at 77 K) is presented in Fig. 1a revealing a type IV isotherm (according to IUPAC classification). Fig. 1b shows the corresponding BET (Brunauer–Emmett–Teller) plot measured using a BELsorp mini II lab analyzer. Based on these, the specific surface area of the silica is determined to be about 615 $m^2$/g. BJH (Barret–Joyner–Halenda) plot of the adsorption branch of the isotherm is presented in Fig. 1c. The curves show that pore size of the synthesized silica falls below 10 nm. This pore size distribution introduces this template as an adequate base for synthesizing uniform mesoporous materials (in this work: $WO_3$). TEM image of the synthesized mesoporous silica is shown in Fig. 2.

HRTEM image of $WO_3$ nanoparticles depicted in Fig. 3a shows that $WO_3$ nanoparticles with average size of about 5 nm are formed. Fourier transform pattern of the nanoparticle in Fig. 3b indicate d-spacing of 3.8 Å corresponding to (0 0 1) planes in monoclinic $WO_3$ crystal structure.

As mentioned above, the specific surface area (SSA) of the products determined using BET technique was found to be about 615 $m^2$/g for mesoporous silica template. This lagre surface area was reduced to 43 $m^2$/g for $WO_3$ nanoparticles after cacination and washing the template. Before heat treatment, the specific surface area of the coated template with tungsten containing materials was measured to be around 350 $m^2$/g. This reduction of the surface is a result of surface coverage and filling the porosities by $WO_3$. After calcination and template removal, the surface area is reduced largely due to the fact that $WO_3$ cannot fill all curvatures and porosities of the host material. In addition, 4 h calcination at 570 °C may activate the growth process.

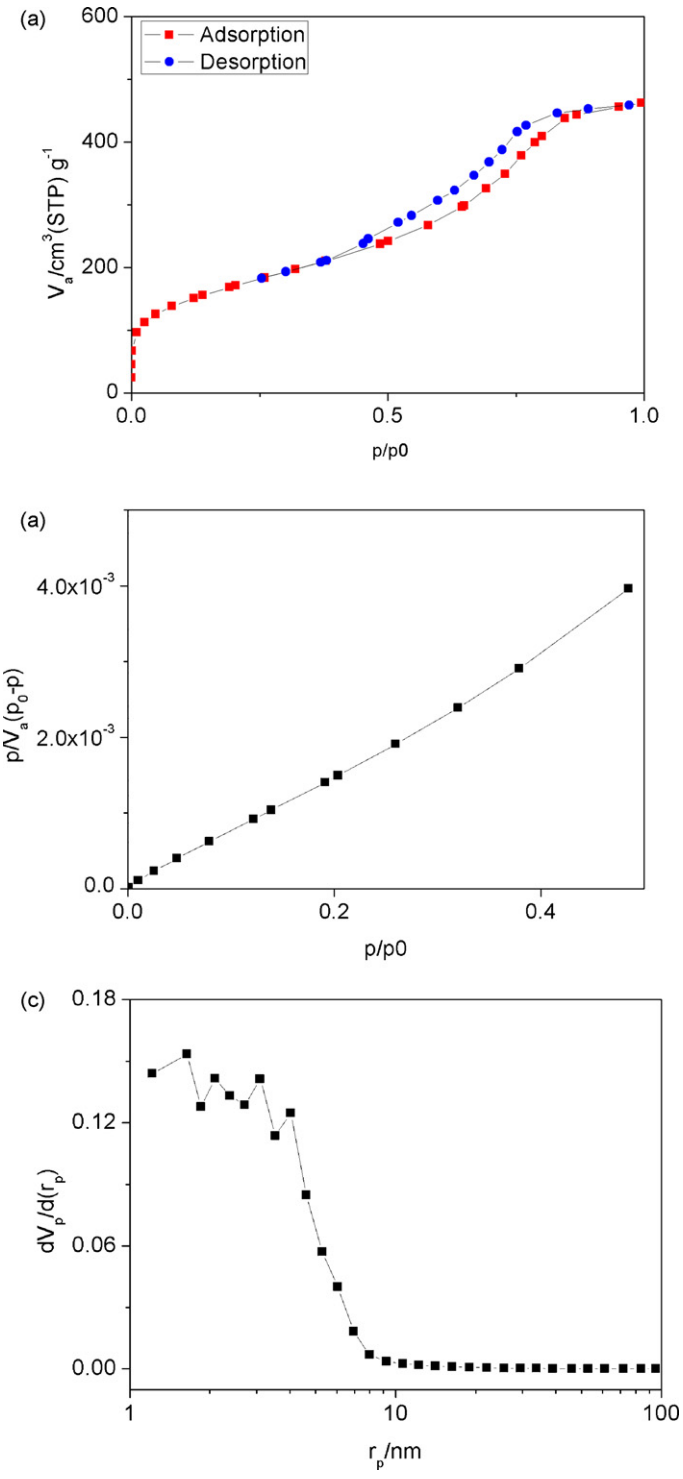


**Fig. 1.** N2 adsorption/desorption isotherm of mesoporous silica showing type IV isotherm (a) and corresponding BET (b); BJH plot of the adsorption branch of the isotherm (c).

Achieving a fully crystalline material with monoclinic crystal structure was verified in XRD patterns obtained for both impregnated template and mesoporous $WO_3$ after template removal (Fig. 4). Washed samples, obviously, present $WO_3$ peaks only. The absence of $SiO_2$ peaks shows that the silica template is completely removed and pure $WO_3$ is remained in the system.

In this research, low frequency AC electrophoresis method is used for sensor fabrication, a simple and reproducible technique

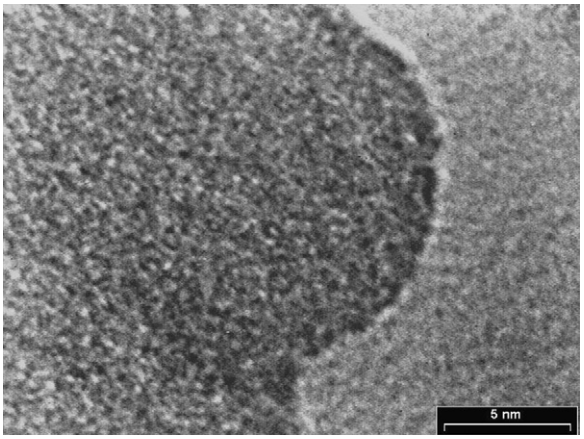


**Fig. 2.** TEM image of mesoporous $SiO_2$ template.

for controlled-manipulation of ceramic nanoparticles and their alignment. Process parameters such as applied voltage, frequency, suspending media, and concentration of particles in suspension can be designed in such a way that the particles migrate toward the gap between two electrodes and deposit there. Particles are deposited on both electrodes simultaneously and the deposited layer grows

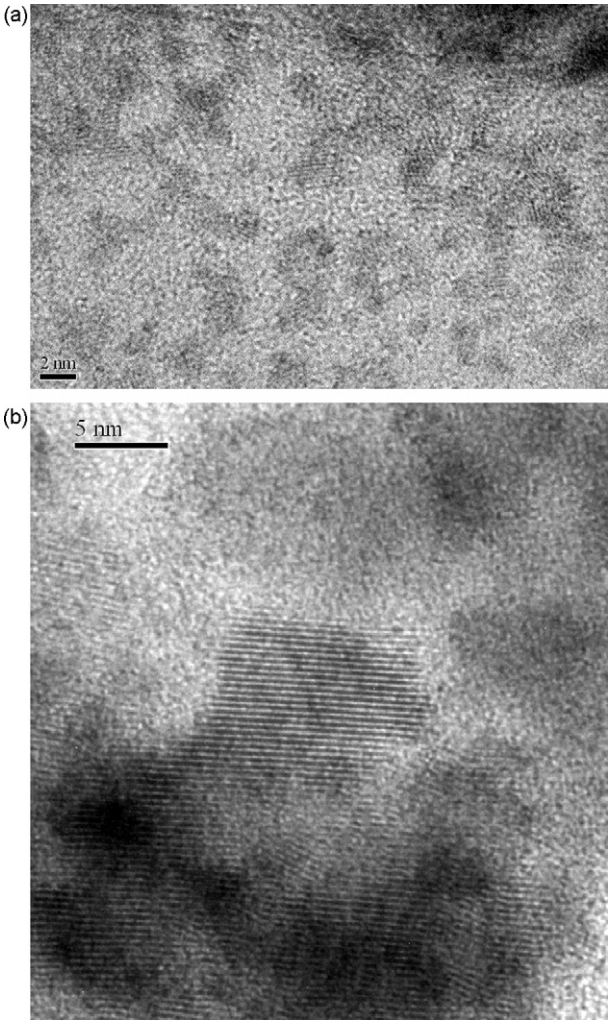


**Fig. 3.** HRTEM image of $WO_3$ nanoparticles array as (a) a replica of silica template and (b) a single $WO_3$ nanoparticle.

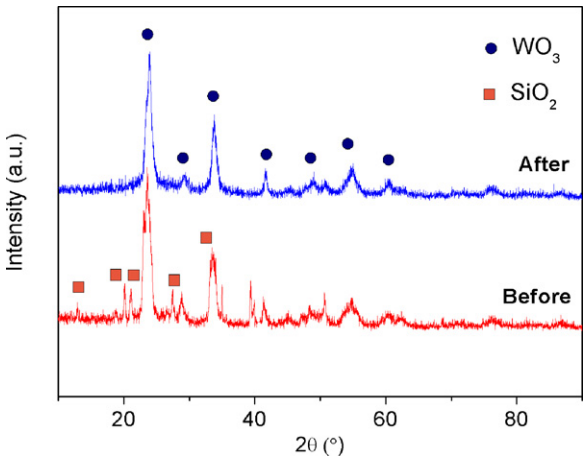


**Fig. 4.** XRD pattern of synthesized $WO_3$ with, and without template indicating the successful impregnation and complete template removal.

from electrodes toward the center of the gap until the gap is filled. Under optimum conditions, particles can bridge between the two electrodes leaving a porous and uniform thick film between them which is an excellent structure for sensing thanks to the pathways facilitating gas flow.

Deposition process is visualized in Fig. 5 through SEM images corresponding to different stages of pattern formation. Fig. 5a is a SEM image of the deposited particles when deposition is ongoing. As it is seen in this figure, $WO_3$ nanoparticles are precipitated on both electrodes and bridged them in some locations. Other bridges are to be formed between the electrodes.

Continued deposition results in a gap fully filled with nano particles (Fig. 5b). An overall view of the sensor is shown in Fig. 5c and d where deposited particles are seen in green color.

Response of the sensor toward various concentrations of $NO_2$ was recorded using a conventional gas sensing setup (Fig. 6). Measurements were performed in the temperature range of 150–300 °C.

Response transients of the sensor at 250 °C presented in Fig. 7 show the clear response of the sensor to the target gas. Obviously, the deposited material behaves in a stable way when exposed to $NO_2$ showing no oscillation in resistance. Moreover, resistance of the sensors recovers its original value (air level) after switching back to the base gas (air) presenting a fully reversible character.

Sensor transients to 500 ppb $NO_2$ at different temperatures are shown in Fig. 8. Responses decrease with increasing temperature while the response/recovery processes take shorter times due to faster kinetics of the adsorption process. $NO_2$ is adsorbed on $WO_3$ surface through the following reversible reaction:

$$NO_2 + e^- \leftrightarrow NO_2^- \quad (1)$$

where electrons are provided by $WO_3$ material. As the above-mentioned chemisorption reaction occurs at the surface, the sensing material is depleted in the surface and as a consequence, resistance increases when the sensor is exposed to the target gas.

At elevated temperatures, the adsorption of gas species on the surface is quite limited so that the reversibility of the process is lost largely and thus, the sensitivity decreases. Adsorption mechanisms are already presented [26] and are not discussed here.

Response and recovery times (defined as time needed to reach 90% of the response or 90% of the original level, respectively) are listed in Table 1 and show that with increasing temperature in the range of 150–300 °C, the response time changes from 22.5 to 7 min and the time needed for recovery decreases from 22.5 to 4.5 min. Although these values are rather long, the high stability in signals can be considered as an advantage of the sensor which is a usual

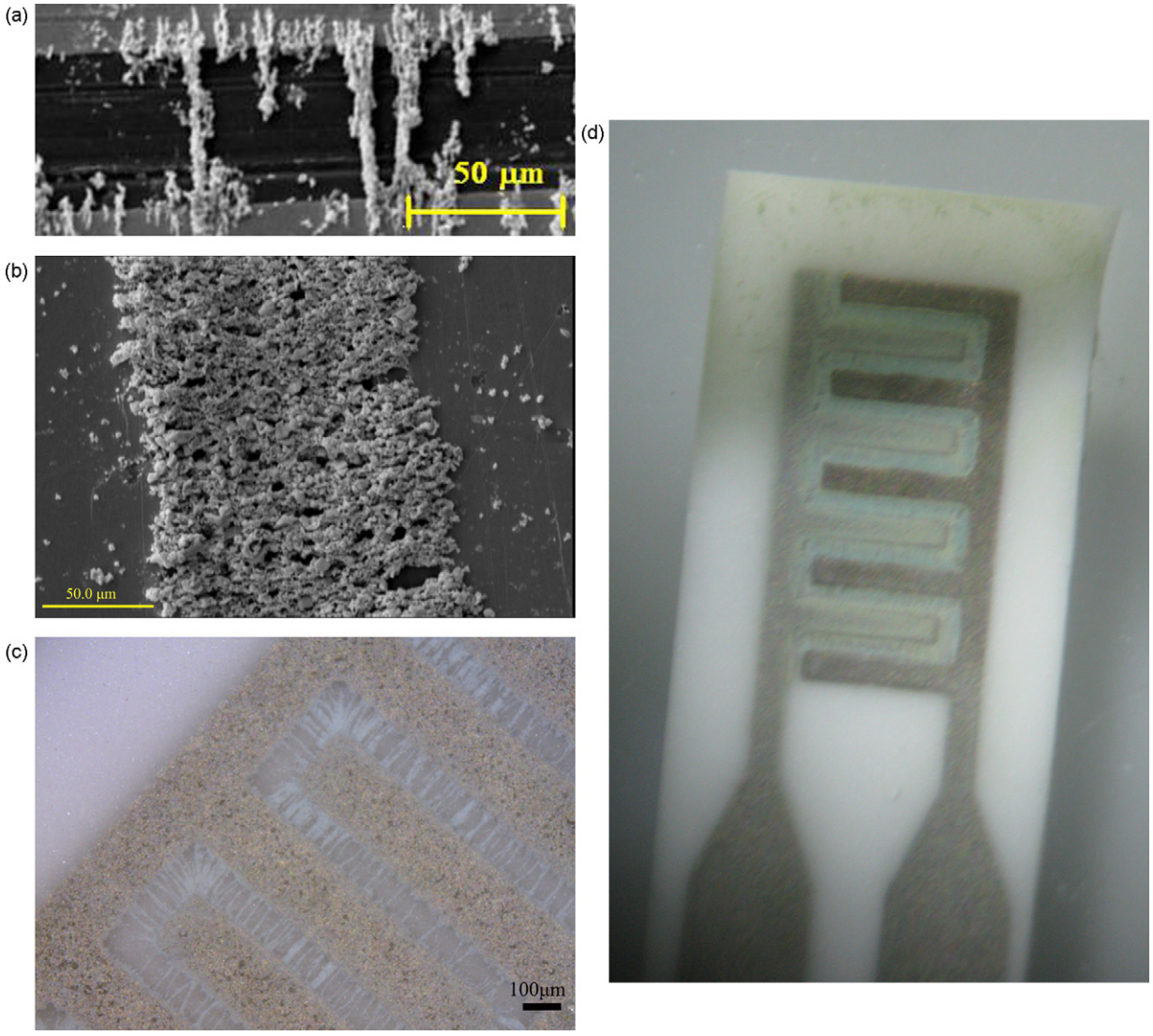


**Fig. 5.** Deposition pattern in different stages: (a) nanoparticles deposited and bridge between electrodes (b) after 60 min, nanoparticles fill the gap, (c) and (d) optical microscopy images of the sensor in which $WO_3$ nanoparticles appear in green color. (For interpretation of the references to color in this figure legend, the reader is referred to the web version of the article.)

problem of this family of chemical sensors. Response and recovery times are determined by adsorption and desorption processes occurring on the surface of the sensing material. This sharp decrease in response and recovery times indicates the facile kinetics of the surface reactions and thus diminished adsorption resulting into lower sensitivity at higher temperatures.

Values of the responses plotted in Fig. 9 confirm the high sensitivity of the device which is comparable to many other pre-

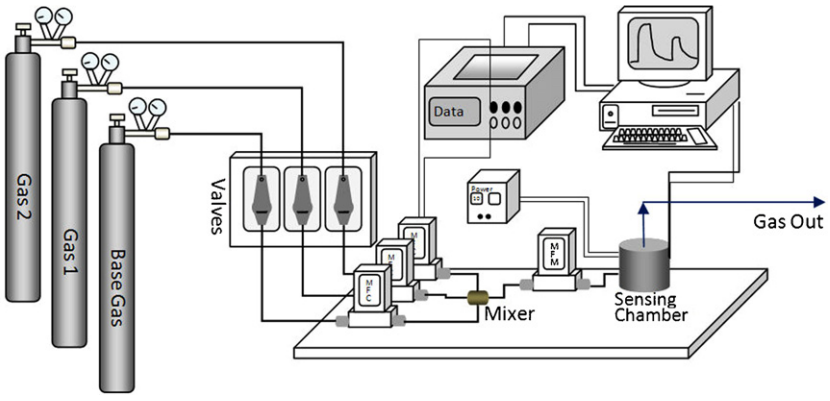


**Fig. 6.** Gas sensing setup used in this study.

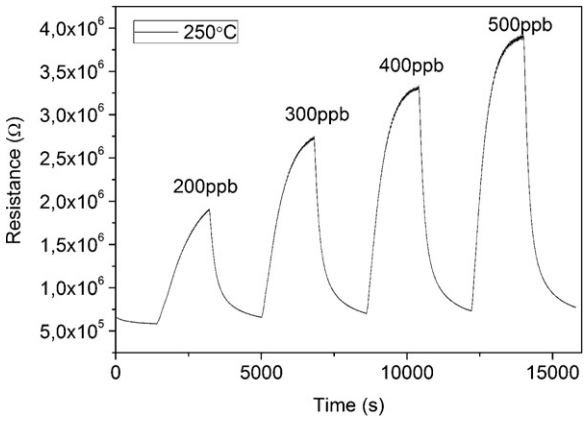


**Fig. 7.** Response transients of the sensor towards 200–500 ppb $NO_2$ at 250 °C.

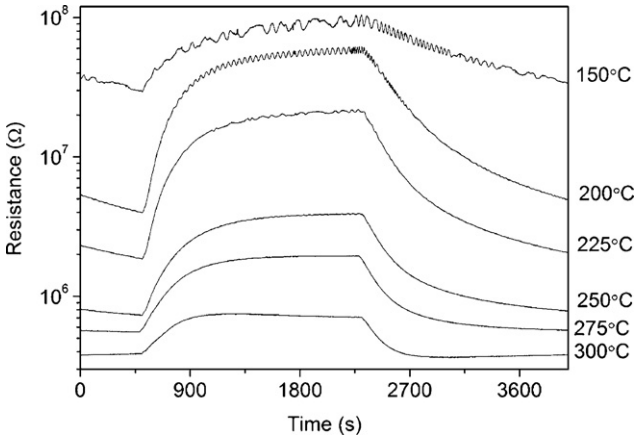


**Fig. 8.** Response transients to 500 ppb $NO_2$ in the range of 150–300 °C.

**Table 1**
Comparison of the sensing properties of the device.

| $T$ (°C) | Response time (min) | Recovery time (min) | Detection range (ppb) |
|---|---|---|---|
| 300 | 7 | 4.5 | 75–500 |
| 275 | 12.5 | 9.5 | 75–500 |
| 250 | 17 | 12.5 | 75–500 |
| 225 | 20 | 13 | 75–500 |
| 200 | 20 | 13.8 | 50–500 |
| 150 | 22.5 | 22.5 | 50–150 |

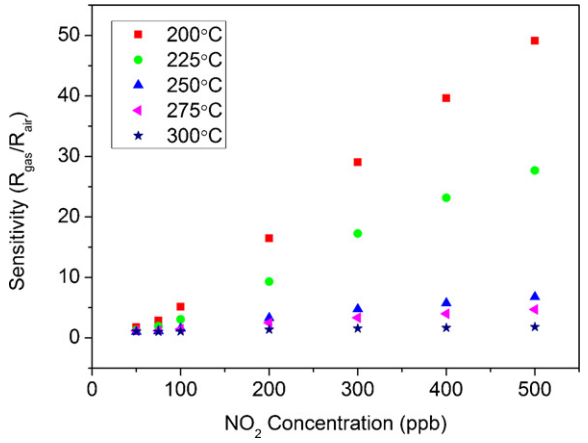


**Fig. 9.** Device sensitivity to various $NO_2$ concentrations revealing linearity in 75–500 ppb gas in the whole temperature range.

viously reported $NO_2$ sensors although some recent works report extraordinary responses [18,26]. A linear trend is obviously seen for all temperatures and concentrations of 100 ppb and above. At higher temperatures the sensor tends to behave linearly in the whole temperature range though at these temperatures (250 °C and above), the sensor response drops drastically. This advantage can be attributed to the unique sensor structure with deposited mesoporous material which in addition to the large surface area, benefits its uniformity and alignment of the particles in the structure. In fact, as it is already reported by Wang et al. [27], in addition to the particle itself, the heterogeneous structure of the deposited layer is also an important sensitivity-controlling parameter. Moreover, Tamaki et al. [18] showed that application of nanoelectrodes in $NO_2$ sensors can increase their sensitivity to a large extent thanks to the increased contact between the material and electrodes. In an excellent review by Korotcenko [17], dimensional factors (which affect sensing properties of the devices) were listed. They have also reported a list of all structural parameters of metal oxides which can affect/control the gas sensing. For thick- and thin films, and also for those sensors fabricated through microdropping of the sensing material, the gas diffusion into the structure has been always a bottleneck of the device limiting the sensitivity to the small surface layer. In the case of the sensor presented here, however, the mesoporous material which inherently possesses a large specific surface area, provides the path for gas flow and surface adsorption. On the other hand, the low frequency electrophoretic deposition, as it was presented in SEM images, leads to a well-structured thin film of the material facilitating sensing process.

## 4. Summary

Tungsten oxide nanoparticles were synthesized and characterized using high resolution TEM. The product was deposited on microelectrodes via low frequency electrophoretic deposition method and used as $NO_2$ sensor presenting a stable device sensitive to $NO_2$ in a dilute range. Response measurements performed in the temperature range of 150–300 °C show that with increasing temperature, the kinetics of the reactions is enhanced and faster response and recovery is observed. However, a lower sensitivity is seen at higher temperatures due to decreased adsorption at these temperatures. Sensor stability was not investigated and is left for further work.

## References

[1] V.M. Aroutiounian, Semiconductor NOx sensors, International Scientific Journal for Alternative Energy and Ecology 4 (48) (2007) 63–76.
[2] N. Miura, M. Ono, K. Shimanoe, N. Yamazoe, A compact solid-state amperometric sensor for detection of $NO_2$ in ppb range, Sensors and Actuators B 49 (1998) 101–109.
[3] S. Nakata, K. Shimanoe, N. Miura, N. Yamazoe, Field effect transistor type $NO_2$ sensor combined with $NaNO_2$ auxiliary phase, Sensors and Actuators B 77 (2001) 512–516.
[4] C. Zamani, K. Shimanoe, N. Yamazoe, A new capacitive-type $NO_2$ gas sensor combining an MIS with a solid electrolyte, Sensors and Actuators B 109 (2005) 216–220.
[5] C. Zamani, K. Shimanoe, N. Yamazoe, Capacitive-type gas sensors combining silicon semiconductor and $NaNO_2$-based solid electrolyte for $NO_2$ detection, Sensors and Actuators B 109 (2005) 300–306.
[6] K. Obata, S. Matsushima, NASICON-based $NO_2$ device attached with metal oxide and nitrite compound for the low temperature operation, Sensors and Actuators B 130 (2008) 269–276.
[7] A.M. Ruiz, G. Sakai, K. Shimanoe, J.R. Morante, N. Yamazoe, Preparation of Cr doped $TiO_2$ thin film of p-type conduction for gas sensor application, Chemistry Letters 31 (2002) 892–983.
[8] M. Akiyama, Z. Zhang, J. Tamaki, N. Miura, N. Yamazoe, Tungsten oxide-based semiconductor sensor for detection of nitrogen oxides in combustion exhaust, Sensors and Actuators B: Chemistry 14 (1993) 619–620.
[9] G. Sberveglieri, P. Benussi, G. Coccoli, S. Groppelli, P. Nelli, Reactively sputtered indium tin oxide polycrystalline thin films as NO and $NO_2$ gas sensors, Thin Solid Films 186 (1990) 349–360.

[10] G. Sberveglieri, L. Depero, S. Groppelli, P. Nelli, $WO_3$ sputtered thin films for NOx monitoring, Sensors and Actuators B 26–27 (1995) 89–92.
[11] T. Inoue, K. Ohtsuka, Y. Yoshida, Y. Matsuura, Y. Kajiyama, Metal oxide semiconductor $NO_2$ sensor, Sensors and Actuators B 24–25 (1995) 368–391.
[12] Y. Yamada, M. Ogita, Transient response of resistive-type $NO_2$ sensor on temperature change, Sensors and Actuators B 93 (2003) 546–551.
[13] Z. Liu, M. Miyauchi, T. Yamazaki, Y. Shen, Facile synthesis and $NO_2$ gas sensing of tungsten oxide nanorods assembled microspheres, Sensors and Actuators B 140 (2009) 514–519.
[14] Y.-G. Choi, G. Sakai, K. Shimanoe, N. Yamazoe, Wet process-based fabrication of $WO_3$ thin film for $NO_2$ detection, Sensors and Actuators B 101 (2004) 107–111.
[15] C. Zamani, O. Casals, T. Andreu, J.R. Morante, A. Romano-Rodriguez, Detection of amines with chromium-doped $WO_3$ mesoporous material, Sensors and Actuators B 140 (2009) 557–562.
[16] M. Tiemann, Porous metal oxides as gas sensors, Chemistry: A European Journal 13 (2007) 8376–8388.
[17] G. Korotcenkov, The role of morphology and crystallographic structure of metal oxides in response of conductometric-type gas sensors, Materials Science and Engineering R 61 (2008) 1–39.
[18] J. Tamaki, T. Hashishin, Y. Uno, D.V. Dao, S. Sugiyama, Ultrahigh-sensitive $WO_3$ nanosensor with interdigitated Au nano-electrode for $NO_2$ detection, Sensors and Actuators B 132 (2008) 234–238.
[19] L.G. Teoh a, Y.M. Hona, J. Shieh b, W.H. Lai a, M.H. Hon, Sensitivity properties of a novel $NO_2$ gas sensor based on mesoporous $WO_3$ thin film, Sensors and Actuators B 96 (2003) 219–225.
[20] A.R. Gardeshzadeh, B. Raissi, E. Marzbanrad, H. Mohebbi, Fabrication of resistive CO gas sensor based on $SnO_2$ nanopowders via low frequency AC electrophoretic deposition, Journal of Materials Science: Materials in Electronics 20 (2009) 127–131.
[21] A.R. Gardeshzadeh, B. Raissi, E. Marzbanrad, Electrophoretic deposition of $SnO_2$ nanoparticles using low frequency AC electric fields, Materials Letters 62 (2008) 1697–1699.
[22] A.R. Gardeshzadeh, B. Raissi, E. Marzbanrad, Preparation of Si powder thick films by low frequency alternating electrophoretic deposition, Journal of Material Science 43 (2008) 2507–2508.
[23] E. Kamali Heidari, E. Marzbanrad, C. Zamani, B. Raissi, Nanocasting synthesis of ultrafine WO3 nanoparticles for gas sensing applications, Nanoscale Research Letters 5 (2010) 370–373.
[24] E. Rossinyol, J. Arbiol, F. Peiró, A. Cornet, J.R. Morante, B. Tian, T. Bo, D. Zhao, Nanostructured metal oxides synthesized by hard template method for gas sensing applications, Sensors and Actuators B 19 (2005) 57–63.
[25] E. Rossinyol, A. Prim, E. Pellicer, J. Arbiol, F. Hernández-Ramírez, F. Peiró, A. Cornet, J.R. Morante, L.A. Solovyov, B. Tian, T. Bo, D. Zhao, Synthesis and characterization of chromium-doped mesoporous tungsten oxide for gas-sensing applications, Advances in Functional Material 17 (2007) 1801–1806.
[26] T. Kida, A. Nishiyama, M. Yuasa, K. Shimanoe, N. Yamazoe, Highly sensitive $NO_2$ sensors using lamellar-structured $WO_3$ particles prepared by an acidification method, Sensors and Actuators B 135 (2009) 568–574.
[27] S.-H. Wang, T.-C. Chou, C.-Ch. Liu, Nano-crystalline tungsten oxide $NO_2$ sensor, Sensors and Actuators B 94 (2003) 343–351.

## Biographies

**Elham Kamali Heidari** was born in Mashhad, Iran in 1984. She received her BSc in Materials Science from Ferdowsi University of Mashhad in 2007. Now, she is a MSc student of Nanomaterials at Materials and Energy Research Center (MERC), Iran working on synthesis of mesoporous materials for gas sensing applications.

**Cyrus Zamani** received his BSc (1997) and Master (1999) degree from Shiraz University, Iran. He obtained his PhD (2005) from Kyushu University, Japan working on semiconductor gas sensors. He worked at RMRC, Iran before starting his work at the University of Barcelona, Spain focusing on integrated gas-chromatographic systems. He also, has collaboration with MERC, Iran in nanotechnology and nanomaterials. He has been author and co-author of several articles on chemical sensors.

**Ehsan Marzbanrad** has been an Assistant Professor at Materials and Energy Research Center (MERC), Iran since 2006. He received PhD degree in Advance Materials in 2004 from Tarbiat Modares University and has been author and co-author of several publications in the field. His research interests include chemical sensors, nanomaterials synthesis, and modeling and simulation.

**Babak Raissi** was born in Tehran, 1963. As Associate Professor of Materials Science, he is working on synthesis and electrophoretic deposition of nanomaterials at Ceramic Department of Materials and Energy Research Center (MERC), Iran. He has authored several articles in the field of electrophoretic deposition of nanomaterials in international journals.

**Soroush Nazarpour** received his BSc in materials science and engineering from Sahand University of Technology, Tabriz, Iran, and his MSc in nanoscience and nanotechnology from the University of Barcelona working on metallic thin films. Now he is a PhD student of nanoscience and nanotechnology continuing his career in thin films for gas sensing applications.